deviation of parameter variations, Δf, is chosen to be sufficiently large.

In order to check the stability of the discrete $TVCNF_1$, its difference equation was solved by a sequential procedure using a digital computer for $\alpha = 0.999$ and $f_0 = 0.1$. The frequency F was increased from $F = 10^{-2}$ up to $F = f_0 = 0.1$. For each F the values of Δf for which the system becomes unstable was found. Fig. 1 shows the results obtained. There exist unstable regions represented by shaded zones. It is seen that in order to get oscillations for low F a large Δf is needed. Such a relationship between F and Δf also follows from the analysis of the Mathieu equation[3] as well as the fact that there exist such frequencies F for which the system is stable even for large Δf.

Filter with two controlled coefficients—$TVCNF_2$: As shown in Reference 4, to reject any sine signal with a time varying frequency, given by $A\cos[\psi(k)+\phi]$, the two coefficients of $TVCNF_2$ have to be functions of the instantaneous phase $\psi(k)$

$$a_1(k) = -\frac{\sin[\psi(k)-\psi(k-2)]}{\sin[\psi(k-1)-\psi(k-2)]}$$

$$a_2(k) = -\frac{\sin[\psi(k)-\psi(k-1)]}{\sin[\psi(k-1)-\psi(k-2)]} \quad (4)$$

with $0 < \psi(k-1) - \psi(k-2) < \pi$ as we are dealing with positive frequency less than π.

Our goal is to check whether $TVCNF_2$ described by eqn. 1 and having the coefficients given by eqn. 4 is asymptotically stable, i.e., to check if the output response of the unforced system (AR part of eqn. 1) approaches zero as $k \to \infty$, for any arbitrary initial conditions. For that purpose let us consider an exponentially damped FM signal

$$y(k) = A\alpha^{(k-k_0)}\cos[\psi(k)+\phi] \qquad k > k_0 \quad (5)$$

It can be proved by constructing an augmented Casarati's determinant associated with $y(k)$, that all independent solutions of the difference eqn. 1 with coefficients given by eqn. 4 may be derived from eqn. 5. The values of A and ϕ in eqn. 5 depend on the initial conditions $y(k_0-2)$ and $y(k_0-1)$. It follows from eqn. 5 that $y(k) \to 0$ for $k \to \infty$ for any A and ϕ, and therefore for any initial conditions, i.e., the system is asymptotically stable. It is interesting to see that $TVCNF_2$ even though is a stable system may have 'poles' lying outside the unit circle. This is not surprising since the concept of poles, developed for time-invariant systems, can not be generally applied to time-varying systems.

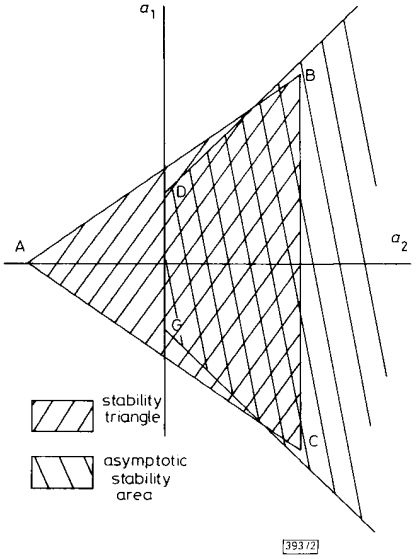

Fig. 2 *Asymptotic stability area and stability triangle*

Consider a structural relationship between $a_1(k)$ and $a_2(k)$ which follows from eqn. 4

$$a_1(k) = -\cos[\psi(k)-\psi(k-1)] + \cos[\psi(k-1)-\psi(k-2)]a_2(k), \quad a_2(k) > 0 \quad (6)$$

From eqn. 6 the structural constraines are obtained

$$|a_1(k)| \le 1 + a_2(k), \qquad a_2(k) > 0 \quad (7)$$

The conditions of eqn. 7 are sufficient conditions for asymptotic stability and may be represented by the asymptotic stability area—the area between two semi-infinite lines which start at points D and G respectively and the axis a_1, as shown in Fig. 2. A stability triangle ABC,[5] which determines the stability of time-invariant system, is also shown for comparison purposes. As expected, the asymptotic stability area and the stability triangle overlap but do not coincide.

Conclusion: Stability of second order TVCNFs, which are capable of rejecting a sine signal with time-varying frequency, was analysed. If the coefficients $a_1(k)$ and $a_2(k)$ of $TVCNF_2$ are found as functions of the instantaneous phase of the sine signal, then using the relationships between them it is proved that $TVCNF_2$ is asymptotically stable. On the other hand, it is shown that the AR-part of $TVCNF_1$ can be explicitly described by the Mathieu equation and therefore such a filter possesses unstable regions, i.e., becomes generally unstable. This fact explains why, for processing a sine signal with time varying frequency (FM), CANF with two controlled coefficients is always preferable to a CANF having only one coefficient.

D. WULICH
E. I. PLOTKIN
M. N. S. SWAMY

Department of Electrical and Computer Engineering, Concordia University, 1455 DeMaisonneuve Blvd., Montreal, Quebec H3G 1M8, Canada

17th May 1990

References

1 RAO, D. V. B., and KUNG, S. Y.: 'Adaptive notch filtering for the retrieval of sinusoids in noise', *IEEE Trans.*, 1984, **ASSP-32**, pp. 791–802
2 NEHORAI, A.: 'A minimum parameter adaptive notch filter with constrained poles and zeros', *IEEE Trans.*, 1985, **ASSP-33**, pp. 983–996
3 RICHARDS, J. A.: 'Modeling parametric processes—a tutorial review', *Proc. IEEE*, 1977, **65**, pp. 1549–1557
4 WULICH, D., PLOTKIN, E. I., and SWAMY, M. N. S.: 'Synthesis of discrete time varying null filters for frequency varying signals using the time warping technique', *IEEE Trans.*, 1990, **CAS-37**, (to be published).
5 SHYNK, J. J.: 'Adaptive IIR filtering', *IEEE ASSP Magazine*, 1989, pp. 4–21

MAXIMUM BITRATE-LENGTH PRODUCT IN THE HIGH DENSITY WDM OPTICAL FIBRE COMMUNICATION SYSTEM

Indexing Optical communications, Raman scattering

The bitrate-length product in the high density WDM optical fibre communication system is analysed by numerical simulation in which both dispersion and Raman crosstalk are considered, and the maximum bitrate-length product is obtained under certain constraints.

In a wavelength division multiplexed (WDM) optical fibre communication system, the bitrate-length product NBL (N: channel number, B: bitrate for a single channel, L: propagation length) measures the capacity of the systems. In this letter we use computer simulation to find the maximum NBL product under certain constraints.

In the analysis, we do not consider any nonlinear effects except Raman crosstalk between channels. In order to get the maximum NBL value, dispersion-shift fibre is used whose zero dispersion wavelength λ_0 is shifted to 1·55 μm. The loss coefficient is assumed to be constant. Here we also assume that the polarisation of the fibre is maintained and the laser source is monochromatic.

The differential equations governing the signal propagation are given by[1,2]

$$\left(\frac{\partial}{\partial z}+\frac{1}{v_i}\frac{\partial}{\partial t}\right)A_i(z,t)=\left[-\frac{\alpha}{2}+\sum_{j=1}^{i-1}\frac{g_{ij}}{2A_{eff}}|A_j(z,t)|^2 - \sum_{k=i+1}^{N}\frac{\lambda_k}{2\lambda_i}\frac{g_{ik}}{A_{eff}}|A_k(z,t)|^2 - i\frac{\beta_i''}{2}\frac{\partial^2}{\partial t^2}+\frac{\beta_i'''}{6}\frac{\partial^3}{\partial t^3}\right]A_i(z,t) \quad (1)$$

where the subscript $i = 1, 2, \ldots, N$ denotes the ith channel, and v, λ, A are the group velocity, wavelength and slowly varying amplitude of the electric field intensity, respectively, β'' and β''' are the first and second order dispersion coefficients. g_{ij} is the Raman gain constant coupling the ith and jth channels, α is the loss constant and A_{eff} is the effective core area. In our analysis, we assume $\alpha = 0{\cdot}18$ dB/km and $A_{eff} = 6{\cdot}36 \times 10^{-11}$ m^2. We also assume that $\lambda_1 < \lambda_2, \ldots, < \lambda_N$ and the N channels are placed symmetrically at the both side of λ_0 with equal channel spacing $\Delta\lambda$. In order to calculate g_{ij} we use a near triangle function (solid curve in Fig. 1) to approximate

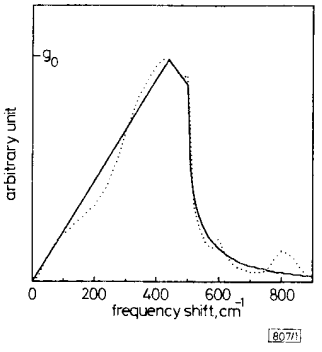

Fig. 1 *Measured and fitted Raman gain profile*
····· measured curve
——— fitted curve

the actual Raman gain profile of silica (dashed curve in Fig. 1), i.e., the peak Raman gain, g_0, occurs at 440 cm^{-1}. For the frequency separation larger than 500 cm^{-1} the Raman gain curve drops as an exponential decay function.

Several criterion are used in our analysis to set up the system model. The minimum detectable energy at the output end is 10^4 photons[3] (about $1{\cdot}3 \times 10^{-15}$ Joules). When the channel spacing $\Delta\lambda$ is larger than the modulation spectrum width of the signal pulse, the minimum output pulse width for a fixed L is obtained by differentiating the following equation[4] with respect to σ_i:

$$\sigma = \sigma_i\left[1+\left(\frac{\beta''L}{2\sigma_i^2}\right)^2+\frac{1}{2}\left(\frac{\beta'''L}{4\sigma_i^3}\right)^2\right]^{1/2} \quad (2)$$

where σ and σ_i are the root mean square width at the output and input end, respectively. When $\Delta\lambda$ is smaller than the modulation spectrum, the above formula will no longer be useful, because the modulation spectrums of two neighbouring channels must be resolvable in the frequency domain. Here we take $\Delta\lambda$ (nm) as four times of the root-mean-square width of the modulation spectrum ($\cong 2{\cdot}55/\sigma_i$, σ_i in picoseconds). The largest bitrate B to guarantee a clear detection in the time domain is given by[5]

$$B = \frac{1}{4\sigma} \quad (3)$$

Since the channel of the shortest wavelength (the first channel) is degraded most severely by the Raman crosstalk, and the dispersion curve is nearly symmetry in the zero dispersion region, the first channel determines both the bitrate and the propagation length. The signal pulses are assumed to be of Gaussian form with constant energy. For a given channel number, N, and channel spacing, $\Delta\lambda$, eqn. 1 is solved by the split-step Fourier method. Then the maximum propagation length can be obtained by checking the propagation length of the first channel. The maximum NBL product is obtained by using eqns. 2 and 3. Plotting these maximum NBL values as a function of N and $\Delta\lambda$ in Fig. 2, we can find an overall

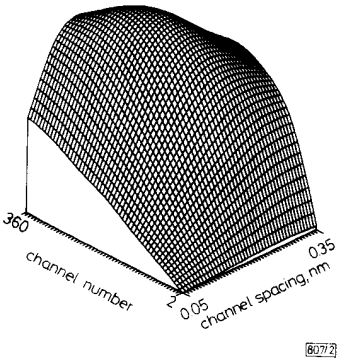

Fig. 2 *Three dimensional diagram of NBL product*

maximum NBL product. In our example, pulses with 10^{-13} joule (about several milliWatt in peak power) are launched, and the maximum value is found to be $3{\cdot}27 \times 10^5$ km Gbit/s at $N = 240$ and $\Delta\lambda = 0{\cdot}2$ nm. It is noticeable that the 3D surface in Fig. 2 composes of infinite 2D curves, and each curve has a local maximum point either for a fixed N (Fig. 3) or for a fixed

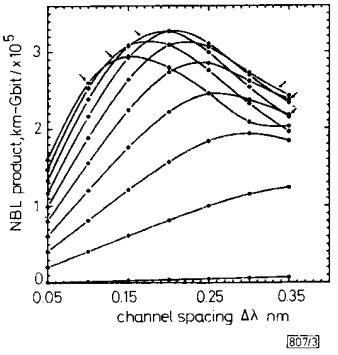

Fig. 3 *NBL product against channel spacing for various channel number*

$\Delta\lambda$ (Fig. 4). The reason for the existence of these local maximum values is that for a fixed channel number, larger $\Delta\lambda$ induces more Raman crosstalk and dispersion and consequently decreases the NBL product. For smaller $\Delta\lambda$ the NBL curve crops owing to the limitation of modulation spectrum. On the other side, for fixed $\Delta\lambda$, larger N induces more Raman crosstalk and dispersion and hence reduces the NBL product, when N is small this degrading effect is not evident and is less than the increasing rate of N, the NBL product increases as N increases.

It was also found that if we change the launching energy and repeat the same procedure we will obtain a set of 3D surfaces as in Fig. 2. The maximum NBL product of each surface changes as the launching energy changes and we can get a optimum launching energy for the NBL product. In summary, if we fix any two of the parameters channel number, channel spacing, and launching energy we can obtain a concave down curve as in Fig. 3 or Fig. 4. This conclusion is applicable not only for the constant loss assumption but is

also applicable for the wavelength dependent loss. The difference between these two cases is that the *NBL* curve goes

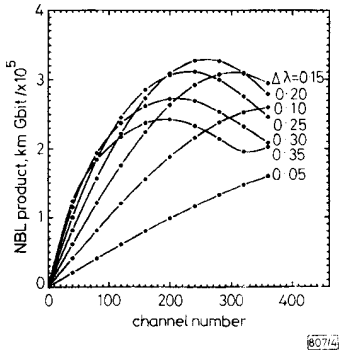

Fig. 4 *NBL product against channel number for various channel spacing*

sharper in the latter one and the position of zero dispersion wavelength λ_0 will play an important role.

S. CHI
S.-C. WANG

Institute of Electro-Optical Engineering and Centre for Telecommunications Research,
National Chiao Tung University,
Hsinchu, Taiwan, Republic of China

17th July 1990

References

1 AGRAWAL, G. P.: 'Nonlinear fibre optics'. (Academic Press, New York, 1989), pp. 218–228
2 KAO, M. S., and WU, J. S.: 'Signal light amplification by stimulated Raman scattering in an N-channel WDM optical fibre communication system', *J. Lightwave Technol.*, 1989, **LT-7**, pp. 1290–1299
3 OSTROWSKY, D. B., and SPITZ, E. (Ed.): 'New directions in guided wave and coherent optics'. (Martinus Nijhoff, 1984), pp. 43–60
4 MARCUSE, D.: 'Pulse distortion in single-mode fibers', *Appl. Opt.*, **19**, pp. 1653–1660
5 NEUMANN, E. G.: 'Single-mode fibers' (Springer-Verlag, 1988), pp. 256–264

UNIFIED APPROACH TO ANALYSE MASS SENSITIVITIES OF ACOUSTIC GRAVIMETRIC SENSORS

Indexing terms: Acoustic transducers, Sensitivity

A unified approach based on Rayleigh's hypothesis for evaluating the mass sensitivities, S_m, of bulk, surface, plate and thin rod flexural acoustic gravimetric sensors is presented. The estimation of S_m uses the 'equivalent depth' which is determined by the displacement distribution of the acoustic mode. The S_m's for the lowest order torsional and longitudinal mode of a thin rod are reported for the first time.

Introduction: Research and development in the area of integrated acoustic gravimetric sensors based on bulk (BAW),[1] surface (SAW),[2] plate[3] and thin rod[4] flexural acoustic waves has become of increasing interest. In order to have high accuracy and sensitivity, these acoustic sensing devices normally operate in the single mode regime. Thus, the BAW of a bulk material,[1] the SAW of a semi-infinite substrate,[2] the lowest antisymmetric Lamb, A_0,[3,5] and shear horizontal, SH_0,[5,6] modes of a thin plate, and the lowest order longitudinal, L_{01},[5] torsional, T_{01},[5] and flexural, F_{11},[4,5] acoustic modes of a thin rod, which can be excited and received predominantly in a single mode regime, are of interest.

For acoustic gravimetric sensors the oscillator mode is often used.[1-3] With this method, an acoustic resonator is used as the frequency control element for the oscillator circuit. A perturbation in the oscillator frequency is monitored in response to changes caused by the measurands. Using Rayleigh's hypothesis, Lu[1] analysed the dependence of the bulk wave resonator frequency on the mass loading. Martin *et al.*,[6] also used this hypothesis to analyse mass sensitivities S_m's of the gravimetric sensors comprised of SH mode plate wave resonators. In this letter, Rayleigh's hypothesis is further extended to analyse the S_m's of SAW,[2,3] thin plate flexural A_0 acoustic[3] and thin rod F_{11},[4] T_{01} and L_{01} devices.

Rayleigh hypothesis approach: According to Rayleigh's hypothesis[1,6] a mechanical resonant system oscillates at a frequency at which the peak kinetic energy U_k is equal to the peak potential energy U_p in the same volume. The energy that appears as a potential energy at a particular time must be totally converted into a kinetic energy after a quarter cycle. For acoustic gravimetric sensors, if the loaded mass layer is very thin and does not contribute to the elastic property of the resonator, the added mass layer will not store any potential energy during the vibration cycle. The peak kinetic energy of the perturbed system will therefore remain unchanged for the unperturbed resonator.[1,6]

The kinetic energy of a mechanical resonator can be expressed by

$$U_k = \frac{\rho\omega_c^2}{2}\int_V \sum_i |u_i(x_2)|^2\, dV \qquad (1)$$

where $\omega_c = 2\pi f_c$ and f_c is the resonant frequency, ρ is the density of the vibrator material, $u_i(x_2)$ is the displacement of the component polarised in the x_i direction at a position x_2, and V is the volume of the mechanical resonator. Later in the text, x_1, x_2 and x_3 refer to Cartesian X, Y and Z axes or cylindrical R, ϕ and Z axes. The analysis here is restricted to two dimensional structures. We assume that the acoustic field distribution is independent of x for the rectangular structures, and that it is azimuthally symmetric for the rod structures. For the sake of simplicity, the modes with only one displacement component will be discussed. We further assume the y direction to be the propagation direction for bulk waves and the z direction for other wave modes. Based on eqn. 1 the kinetic energy density per unit area on the principal plane for the rectangular structures is

$$U_k = \frac{\rho\omega_c^2}{2}\int_0^d |u(y)|^2\, dy \qquad (2a)$$

where d is the depth of the acoustic energy distribution in the substrate. For SAW devices the integration limit, d, can be replaced by a few wavelengths. The kinetic energy density per unit length for the rod structures can be expressed as

$$U_k = \frac{\rho\omega_c^2}{2}(2\pi)\int_0^d |u(r)|^2 r\, dr \qquad (2b)$$

where a is the radius of the rod and $u(y)$ or $u(r)$ is the displacement distribution of the corresponding mode.

When a mass layer is deposited on the surface of the resonator, and if the loaded layer is very thin so that the mass loading does not alter the distribution of the acoustic fields in the resonator, the kinetic energy density of the perturbed resonator can be expressed by

$$U_k' = \frac{\omega_p^2}{2}\{\rho' h u_0^2 + \rho\int_0^d |u(y)|^2\, dy\} \qquad (3a)$$

for the rectangular structures and

$$U_k' = \frac{\omega_p^2}{2}\{\rho' h u_0^2(2\pi a) + (2\pi)\rho\int_0^a |u(r)|^2 r\, dr\} \qquad (3b)$$